Journal of Anatomy

J. Anat. (2013) **223**, pp159–170 doi: 10.1111/joa.12067

Mineralization of the vertebral bodies in Atlantic salmon (*Salmo salar* L.) is initiated segmentally in the form of hydroxyapatite crystal accretions in the notochord sheath

Shou Wang,[1] Harald Kryvi,[1] Sindre Grotmol,[1] Anna Wargelius,[2] Christel Krossøy,[1] Mattias Epple,[3] Frank Neues,[3] Tomasz Furmanek[2] and Geir K. Totland[1]

[1]*Department of Biology, University of Bergen, Bergen, Norway*
[2]*Institute of Marine Research, Bergen, Norway*
[3]*Inorganic Chemistry and Center for Nanointegration, University of Duisburg-Essen, Essen, Germany*

Abstract

We performed a sequential morphological and molecular biological study of the development of the vertebral bodies in Atlantic salmon (*Salmo salar* L.). Mineralization starts in separate bony elements which fuse to form complete segmental rings within the notochord sheath. The nucleation and growth of hydroxyapatite crystals in both the lamellar type II collagen matrix of the notochord sheath and the lamellar type I collagen matrix derived from the sclerotome, were highly similar. In both matrices the hydroxyapatite crystals nucleate and accrete on the surface of the collagen fibrils rather than inside the fibrils, a process that may be controlled by a template imposed by the collagen fibrils. Apatite crystal growth starts with the formation of small plate-like structures, about 5 nm thick, that gradually grow and aggregate to form extensive multi-branched crystal arborizations, resembling dendritic growth. The hydroxyapatite crystals are always oriented parallel to the long axis of the collagen fibrils, and the lamellar collagen matrices provide oriented support for crystal growth. We demonstrate here for the first time by means of synchroton radiation based on X-ray diffraction that the chordacentra contain hydroxyapatite. We employed quantitative real-time PCR to study the expression of key signalling molecule transcripts expressed in the cellular core of the notochord. The results indicate that the notochord not only produces and maintains the notochord sheath but also expresses factors known to regulate skeletogenesis: *sonic hedgehog* (*shh*), *indian hedgehog homolog b* (*ihhb*), *parathyroid hormone 1 receptor* (*pth1r*) and *transforming growth factor beta 1* (*tgfb1*). In conclusion, our study provides evidence for the process of vertebral body development in teleost fishes, which is initially orchestrated by the notochord.
Key words: collagen; hydroxyapatite; mineralization; notochord; salmon.

Introduction

The notochord ensures structural stability and acts as an anchor point for muscle contraction at some stage of development in all vertebrates, being an ancient functional antecedent of the vertebral column. The cells of the differentiated notochord in bony fishes (teleosts) comprise a stratified cellular core made up of an inner part of fluid-filled chordocytes and an outer germinal layer of chordoblasts, encased in a thick fibrous sheath. The external surface of the sheath consists of a continuous layer of elastin (the elastic membrane) covering the thick lamellar collagenous layer. The expansion of the inflatable vacuolated core is restricted by the notochord sheath, and this generates the hydrostatic properties that provide support for the oscillatory swimming movements (Adams et al. 1990; Koehl et al. 2000; Grotmol et al. 2003).

During development, the notochord gives rise to the ossified vertebral column, which is composed of articulated vertebrae with processes in teleosts and tetrapods, including mammals. In teleosts, such as Atlantic salmon (*Salmo salar* L.) and zebrafish (*Danio rerio*), the development of the vertebral body differs fundamentally from that of mammals in its embryonic origin, morphogenesis and patterning process. The formation of vertebral bodies in mammals starts with a cartilaginous anlage that becomes ossified by osteoblasts originating from the somitic sclerotome (endochondral ossification), whereas in teleosts the verte-

Correspondence
Shou Wang, Department of Biology, University of Bergen, Bergen, Norway. E: Shou.Wang@bio.uib.no

Accepted for publication *7 May 2013*
Article published online *27 May 2013*

bral bodies are formed directly in bone (direct ossification) from two different anlagen. The first to appear is the chordacentra, segmental acellular mineralized rings, as an integrated part of the notochord sheath, which on the basis of morphological criteria consists mainly of type II collagen fibrils. The notochord sheath thus shares certain features with cartilage; however, the spatial distribution of the collagen fibrils differs. In the notochord sheath, the collagen fibrils are anisotropic and are organized into distinct layers, each with its fibrils parallel to each other, forming helices around the longitudinal axis of the notochord (Eikenberry et al. 1984; Fleming et al. 2004; Grotmol et al. 2006). In a second developmental step, the chordacentra are surrounded by somite-derived osteoblasts that settle on the elastic membrane, where they deposit osteoid rich in lamellarly organized type I collagen fibrils, soon followed by mineralization. The osteoblasts accumulate in the cranial and caudal rims of the chordacentra. The compact bone thus grows through extension at the rims resulting in the typical hour-glass-like shape of a teleost vertebral body (Grotmol et al. 2005; Nordvik et al. 2005).

Mineralization is a well orchestrated process through which a highly organized arrangement of hydroxyapatite crystals is formed in precise amounts within an extracellular matrix rich in collagen fibrils. Although chemical and physical analyses have revealed details of the structure and organization of mineral in collagen matrices, it is still unclear how calcium and phosphate ions are sequestered from the soluble phase to form crystals. Two main mechanisms of mineral induction have been proposed: 'passive' matrix-regulated model and the 'active' cell-mediated model (Dorozhkin & Epple, 2002; Veis, 2003; Qin et al. 2004; Anderson et al. 2005; Huq et al. 2005; Glimcher, 2006; Boskey, 2007; Zhu et al. 2008; Landis & Silver, 2009; Bonucci, 2012). The matrix-regulated models place the focus of crystal nucleation squarely on the organic matrix and it has been suggested that nucleation takes place within the gap regions of the collagen fibril. The cell-mediated model emphasizes that secretion of minute membrane-bound bodies, known as matrix vesicles, formed by exocytosis from bone-forming cells, mediate and initiate the mineralization process. Thus, by releasing matrix vesicles, cells remotely control and prime extracellular events. How apatite nucleation and accretion are mediated in the collagen matrix is still the subject of dispute.

Atlantic salmon is a well suited model organism for studies of early vertebral column mineralization and bone modelling in vertebrates, due to the advantages of its large notochord and slow early development stages relative to established teleost models such as zebrafish and Japanese medaka (*Oryzias latipes*). Furthermore, the mineralized zones of the vertebral body rudiments are thin, making it possible to cut ultrathin sections of non-decalcified tissue. Potential artefacts that may result from decalcification of bone matrix, possibly obscuring morphological details, are thus eliminated, making it easier to describe the three-dimensional spatial relationship between the mineral crystals and the collagen fibrils.

By forming the initial chordacentrum, the notochord itself nucleates vertebral development, but it has not been fully documented whether the segmental mineralization is controlled by the notochord itself or in combination with outside influences (Bensimon-Brito et al. 2012). We know that the cellular core of the salmon notochord expresses a unique set of structural molecules (Sagstad et al. 2011) but we do not know the origin and identity of the molecules involved in the mineralization process or the exact composition of the chordacentrum. In vertebrates, several factors contribute to the initiation of the conserved process of mineralization. Among them are secreted factors, which include hedgehogs and transforming growth factor betas (TGF-β) but also parathyroid hormone-associated factors such as the parathyroid hormone receptor (Abbink & Glik, 2007; Yu et al. 2012). We do not know whether these factors are active during mineralization of the notochord. However, this study investigated how these molecules are regulated during mineral crystal nucleation and accretion. This has been approached from a morphological point of view by employing high- resolution electron microscopy on non-decalcified samples, and by observing the underlying gene expression of key structural and signalling factors in the cellular core of the notochord from a series of early developmental stages of the Atlantic salmon, encompassing the precursor phase of bone formation when the earliest deposition of mineral matter takes place.

Materials and methods

Stock maintenance and sampling for morphology and crystal identification

Eggs, larvae and juveniles of Atlantic salmon were collected from a local commercial hatchery, where they had been held in a flow-through system (Marine Harvest, Askøy, Norway). Water temperature was kept at 8.0 °C throughout the egg stage until after hatching, when the temperature was raised to 8.5 °C. At start-feeding the temperature was raised to 15.0 °C linearly over a period of 2 days. The fish were fed a commercial feed *ad libitum*. Developmental stages were classified by day degrees (d°), which are defined as the sum of daily mean ambient water temperatures (°C) for each day of development. Hatching occurred at around 500 d°, while first feeding commenced towards the end of the yolk-sac period, at approximately 870 d°. Selected developmental stages up to 2500 d° were analyzed sequentially. Samples of 20 fish from each stage were collected and brought to the laboratory in bags of oxygenated water. Before the preparative procedures, the fish were anaesthetized with 5% benzocaine dissolved in water.

Bone staining of whole mounts

Before staining, the specimens were fixed for at least 48 h in 4% formaldehyde in phosphate buffer (pH 7.4). The fish were immersed

in a buffered enzyme solution for up to 7 days, depending on their size. This solution contained 0.4 mg mL^{-1} of trypsin (Sigma Chemical Co., London, UK), proteinase K (E. Merck, Darmstadt, Germany), pronase (E. Merck) and lipase (Sigma Chemical Co.). They were then washed in buffer and bleached in 0.3% H_2O_2 in 1% KOH for 1–4 h, depending on their size. The bone matrix was then stained with 0.1 mg mL^{-1} Alizarin red S (CI 58005) in 1% KOH for 24–48 h, depending on the size of the sample, and then dehydrated and stored in glycerol.

Transmission electron microscopy (TEM)

Specimens were fixed by immersion in a mixture of 10 mL 10% formaldehyde (fresh from paraformaldehyde), 10 mL 25% glutaraldehyde, 20 mL 0.2 M cacodylate buffer and 60 mL phosphate-buffered saline (PBS), and the pH adjusted to 7.35. They were then rinsed in PBS and in dH_2O, before post-fixation in 1% OsO_4. The specimens were dehydrated in ethanol (70, 90 and 100%) and embedded in Epon 812 (Fluka Chemie AG, Buchs, Switzerland). Ultrathin sections (50 nm) were placed on grids, contrasted with uranylacetate and lead citrate, and viewed in a Jeol 1011 and a Philips CM 200 transmission electron microscope.

Preparation of samples for synchrotron-radiation based X-ray diffraction

Chordacentra and bone from the vertebral body were analyzed. To collect notochord centra, larvae at stage 700 d° were macerated by immersion in 1% KOH for 12 h, chordacentra were stained with Alizarin red S and washed in buffer in order to detect them during collection of samples. More than 18 000 centra were carefully sampled under visual control using an eyelash attached to a thin wood rod. They were then transferred by pipette to Eppendorf tubes, washed in buffer, dehydrated in acetone and dried in a critical point dryer. Bone from the vertebral bodies of intact vertebrae, number 40 counted from the head, was obtained from specimens at developmental stages ranging from 1500–2500 d°. To disconnect soft tissue from the bone, the fish were heated in water to 56 °C, and thereafter cleaned in buffer. The neural and haemal arches were carefully removed by dissection from the vertebral body.

The samples used for high-resolution X-ray powder diffraction were measured in beamline B2 of the DORIS storage ring of Hamburger Synchrotronstrahlungslabor (HASYLAB) at Deutsches Elektronen-Synchrotron (DESY), a Research Centre of the Helmholtz Association, in Hamburg. The synchrotron permitted analysis at high resolution with a low signal-to-noise ratio, which is superior to conventional X-ray diffractometers equipped with X-ray tubes.

The wavelength used was $\lambda = 1.18\,344$ Å and the data were collected by an image plate detector (OBI) in transmission geometry (Knapp et al. 2004a,b). Before measurement, the samples were ground and placed on the kapton foil of the sample holder. A drop of acetone was put on the sample to fix it on the film. The reflections were indexed according to the International Centre for Diffraction Data (ICCD) for hydroxyapatite (#9-0432). The average particle size (approximated as the crystallographic domain size) was calculated by employing the Scherrer equation from different reflections (Becker et al. 2004). Mouse bone and human bone were used as reference tissues (Peters et al. 2000).

$$Scherrer\ equation: FWHM = \frac{K \cdot \lambda \cdot 57.3}{D \cdot \cos(\Theta)}$$

where FWHM is full-width at half maximum in 2θ, K is a constant set to 1 in the procedure (as is usually done), λ is the X-ray wavelength in Å, D is the crystallite size in Å and θ is the diffraction angle of the corresponding reflex in $^{\circ}\theta$.

The samples for thermogravimetric analysis were heated to 1200 °C at a rate of 3 $K\ min^{-1}$ and the mass loss was recorded (Table 1). The content of carbonate (M = 60.01 g mol^{-1}) in hydroxyapatite was calculated from the loss of carbon dioxide (M = 44.01 g mol^{-1}):

$$w\left(CO_3^{2-}\right) = \frac{w(CO_2) \cdot 60.01}{44.01}$$

Dissection of notochord core fractions for gene expression study

Salmon embryos were kept at around 4 °C until sampling. Sampling was done at three developmental stages at 510 d° (± 20 d°), 610 d° (± 20 d°) and 710 d° (± 20 d°). The notochord was dissected out according to a procedure described by Sagstad et al. (2011) and cut into three equal segments from which pure cellular core were extracted out from the sheath. The samples were immediately fresh-frozen on liquid nitrogen and stored at −80 °C until RNA isolation.

RNA isolation and cDNA synthesis

Total RNA was extracted from notochord samples using an RNeasy Mini Kit (Qiagen, Hilden, Germany) according to the instruction manual. The quality and amount of total RNA was controlled by a NanoDrop (ND-1000, Thermo Scientific, Wilmington, DE, USA). Only RNA samples with A260/280 in between 1.8 and 2.0 were accepted for downstream analysis. In total, 12–18 fish larvae at 510 d°, five to eight fish larvae at 610 d° and four fish larvae at 710 d° were pooled as triplicates. For cDNA synthesis a SuperScript VILO cDNA

Table 1 Average crystallite size (nm) in notochord centra and vertebral bodies of Atlantic salmon, determined by high-resolution X-ray powder diffractograms calculated by the Scherrer equation from different X-ray diffraction peaks (hkl). The results are compared with those of mouse and human bone.

	Reflection (hkl)				
	002	310	222	213	004
Diffraction angle (°2θ)	19.8	30.2	35.5	37.5	40.2
Notochord centra (nm)	21.0				
Vertebral body (nm)	21.0	6.3	15.6	12.6	20.5
Mouse bone (nm)	20.9	6.4	6.4	11.5	13.4
Human bone (nm)*	20	8	15	12	18

*Peters et al. (2000).

Synthesis Kit (Invitrogen) was employed in accordance with the manufacturer's guidelines.

Quantitative gene expression analysis

The level of gene expression level in the cellular core of the notochord was analyzed by quantitative real-time PCR (qPCR) using SYBR Green PCR Master Mix (Applied Biosystems Inc., Foster City, CA, USA). PCR reactions were run at 7900HT Fast Real-Time PCR System (Applied Biosystems). The conditions for all reactions were 50 °C for 2 min, followed by 95 °C for 10 min, 40 cycles of 95 °C for 15 s, and 60 °C for 1 min. Genomic fragments from the first released salmon genome assembly (Genebank assembly ID: 313068) were used to design primers and probes. Primers were designed using PRIMER EXPRESS v2.0 software (Applied Biosystems). *Elongation factor 1* α (*ef1a*) was used as reference gene for its stable expression in various salmon tissues (Olsvik et al. 2005) including the notochord (Wargelius et al. 2010; Sagstad et al. 2011). Primer sequences and genomic template are listed in Table 2. Three replicate cDNAs were prepared for gene expressional analysis. A standard curve analysis was performed to confirm the similar amplification efficiency between the target gene and the reference gene with a validation step (Table 2). No template control (NTC) and RNA sample without reverse transcription (–RT) were used to control contamination of external and genomic DNA in reactions. Melting curve analyses were performed on each primer pair to confirm a unique amplicon reaction.

Statistical analysis

All statistical analyses were performed with GRAPHPAD PRISM version 5 (GraphPad Software, San Diego, CA, USA). Samples were grouped according to by developmental stage, for a D'Agostino–Pearson omnibus normality test. For the relative expression value of genes following a Gaussian distribution ($P > 0.05$), one-way ANOVA with Tukey's multiple comparison test was used to reveal which groups were differentially expressed. Genes that did not pass the normality test ($P > 0.05$ in at least one group) were subjected to a nonparametric Kruskal–Wallis test with Dunn's multiple comparison test. Differentially expressed genes were defined as significant if $P < 0.001$ in either one-way ANOVA or Kruskal–Wallis test.

Results

Each chordacentrum forms by the fusion of three bony elements

The ring-shaped chordacentra form segmentally in the outer half of the notochord sheath, starting close to the covering elastic membrane, at around 650 d°. Initially, two ventrolateral patches of bone appear and are followed immediately by a ventral plate-like structure (Fig. 1A). These fuse, initially along the caudal rim (Fig. 1C), to create a ventral, M-shaped bone, with two incisures for the articulation with the haemal arch (Fig. 1D,E). The lateral patches grow in a symmetrical manner with ends pointing in the dorsal direction along the circumference of the sheath (Fig. 1F). The dorsad-growing walls finally fuse (Fig. 1G) to form a complete mineralized ring (Fig. 1H). The chordacentral rings have diameters of 400 μm, are 150 μm long, and the wall is 10 μm thick, located central to the elastic membrane (Fig. 2A). Each chordacentrum persists as the narrow tube in the middle of the mature vertebral body, connecting the notochord tissue along the entire vertebral column. Further growth of the vertebral body occurs mainly external to the elastic membrane, in the sclerotome-derived (type I collagen) compact and spongeous layers of the vertebral body.

Table 2 Primer and amplicon information in quantitative real-time PCR reactions.

Gene symbol	Amplicon (accession)	Primer sequences
col2a1	AGKD01129929	Forward: 5′-ACGGCTGCACGAAACACA-3′ Reverse: 5′-TGGGAGCAATGTCCACGAT-3′
col11a1	AGKD01012341	Forward: 5′-CAACCCCTACATCAGGGCC-3′ Reverse: 5′-CACAGTCTTTCCGTAGCCCTTC-3′
col1a2	CA064459	Forward: 5′-GAGGGTGGATGCAGGTGTGT-3′ Reverse: 5′-TACTGGATCGACCCCAACCA-3′
pth1r	AGKD01141489	Forward: 5′-CAGCAGTACAGGAAGCTGTTGAA-3′ Reverse: 5′-CATAAACACCATATAGTGCACTCCAA-3′
tgfb1	AGKD01178587	Forward: 5′-TGAGTGTGGTAAATCCGAGGAA-3′ Reverse: 5′-TCGTACCCCGCTGTCCAA-3′
shh	AGKD01079961	Forward: 5′-GTCCAAGGCCCACATCCA-3′ Reverse: 5′-GGAAGCAGCCGCCTGAT-3′
ihhb	AGKD01050893	Forward: 5′-CGGAAGGAATTCTACACCATTAGG-3′ Reverse: 5′-TTCCCTCGGACACGAACAG-3′
*ef1a**	AF321836	Forward: 5′-CCCCTCCAGGACGTTTACAAA-3′ Reverse: 5′-CACACGGCCCACAGGTACA-3′

*Olsvik et al. (2005).

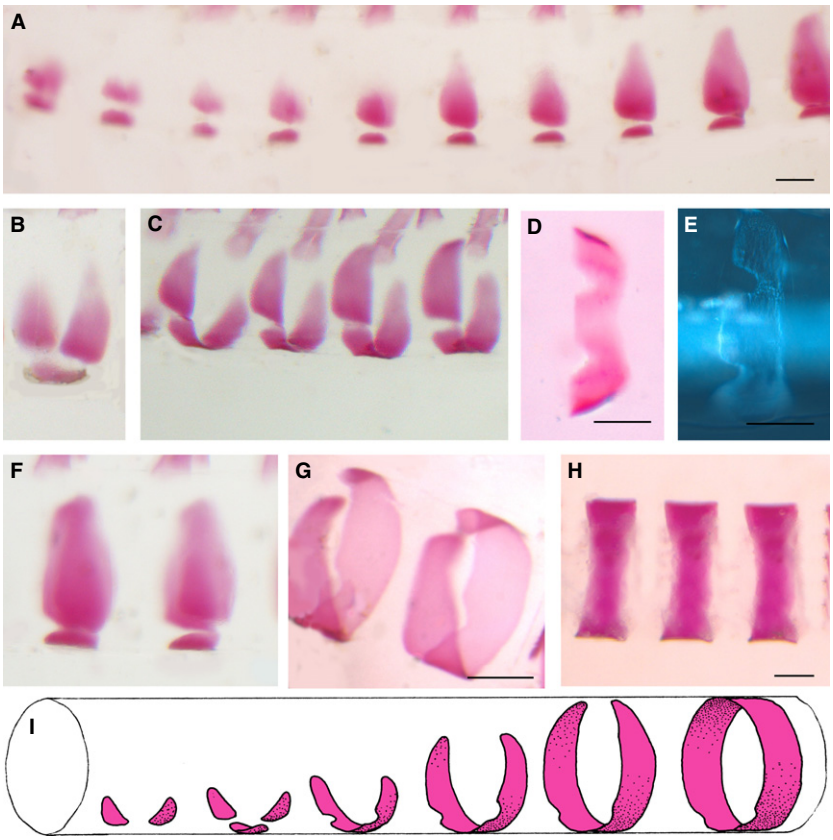

Fig. 1 Formation and growth of the chordacentra inside the notochord sheath, 680–720 d°. Cranial end towards left on all figures. (A,B) Early stage of mineralization, with three separate bony elements, one ventral and two lateral. (A) is lateral view and (B) is oblique lateral view. (C) Oblique lateral view showing the fusion of the three elements, creating an m-shaped bone with incisures for haemal arch articulation, seen in (D,E) ventral views. (F,G) The walls grow and finally fuse dorsally, creating complete rings. (F) Lateral view. (G) Dorsolateral view. (H) A lateral view of the complete rings. (I) Schematic drawing to summarize the sequence of events during chordacentra formation. All specimens are Alizarin-stained whole-mounts except for (E), which is unstained and photographed with DIC microscopy. Scale bars: 150 μm.

Mineralization in the chordacentra starts with thin plate-like structures

The mineralization process that produces the chordacentra, in the type II collagen matrix of the notochordal sheath (Fig. 2A,B), starts with the formation of thin electron-dense platelets, about 5 nm in thickness, in the interfibrillar space between the collagen fibrils (Fig. 2C–G). The specimens were non-decalcified, and the only difference between mineralized and non-mineralized regions of the tissues was the presence of these platelets. Collagen fibrils were always arranged in close proximity to the thin platelets, which were never observed to penetrate the fibrils (Fig. 2C–F). The collagen fibrils are spaced at between 40 and 60 nm separation along the platelets. No rod- or needle-shaped mineral densities were observed in the isolated crystals. During the next stages of growth, the thin platelets aggregate in a seemingly random fashion by the fusion of adjacent platelets (Fig. 2B,G), forming extensive multi-branched crystal arborizations that resemble dendritic growths. The platelets were always arranged parallel to the collagen fibrils, forming complex star-shaped clusters, each about 0.5 μm in diameter (Fig. 2A,B). From transverse sections of the notochord, the true shape of the early crystals, thought to represent the habit of the apatite crystal, was deduced, as the sections are parallel to the collagen fibrils (Fig. 2H,I), for the rare cases where an entire platelet was located within the section. In such cases, the long crystal axes (*c* axes) appear to be approximately parallel to the long-axis direction of the collagen fibrils in areas where the thin sections were also parallel to the long axes of the collagen fibrils. The relationship between collagen fibrils and the early mineral platelet cluster is depicted schematically in Fig. 3, showing a star-shaped cluster of thin crystal plates and closely adjacent collagen fibrils.

Mineralization in the part of the vertebral body that surrounds the chordacentrum (arcocentrum) starts immediately external to the elastic membrane (Fig. 2A) and thus starts to develop with the newly formed chordacentrum as its foundation. In this area, a layer of longitudinal collagen fibrils is surrounded by thicker bundles of circularly organized fibrils, which mineralized simultaneously (Fig. 4A). As Fig. 4(B,C) shows, the earliest crystal platelets nucleate and accrete close to the surface of the collagen fibrils, starting with thin platelets (5 nm thick) that later fuse and produce star-shaped clusters. These are oriented parallel to the collagen fibrils, producing thin, electron-dense lines among the transversely sectioned fibrils, and more diffuse electron-dense patches among the longitudinally sectioned fibrils (Fig. 4A). Eventually, the elastic membrane disappears when the chordacentrum and the autocentrum merge to produce the vertebral body. No matrix vesicles were observed either in the notochord sheath or in the mineralizing osteoid.

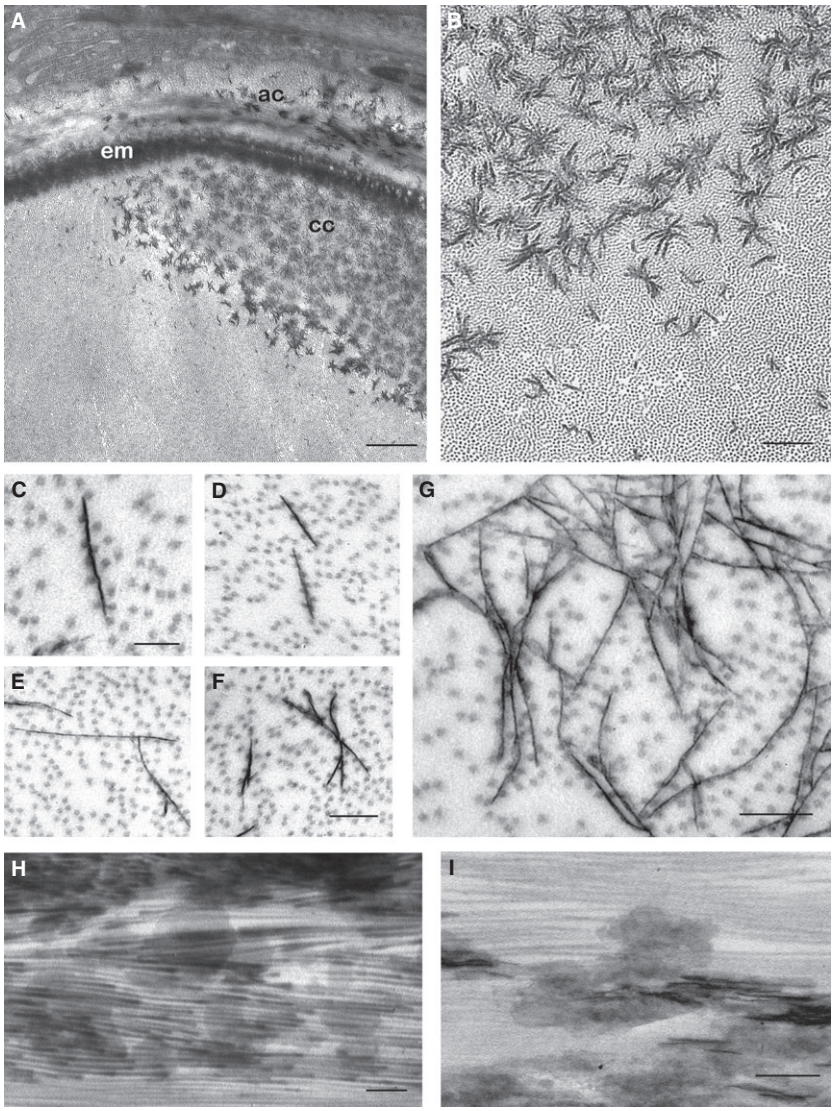

Fig. 2 Mineralization in the chordacentra, 700 d°. Transmission electron micrographs: (A–G) longitudinal sections, (H,I) transverse sections. (A) The edge of the developing chordacentrum (cc), close to the elastic membrane (em). The sclerotome-derived autocentrum (ac) is located external to the elastic membrane. Scale bar: 1 μm. (B) Irregular star-shaped mineral aggregations of the chordacentrum. Scale bar: 500 nm. (C-F) Early mineralization, with electron-dense platelets and associated collagen fibrils. (C,D) Individual unbranched platelets. (E,F) Initiation of dendritic branching and platelet associations. Note the orientation parallel to the collagen fibrils. Scale bars 100 nm (C), 200 nm (F); this scale is valid for (D,E). (G) An early mineral aggregate. Scale bar: 100 nm. (H,I) Transverse section, parallel to the collagen fibrils. Numerous electron-dense platelets with relatively regular shapes are seen. Scale bars: 100 nm.

The chordacentrum is composed of a carbonate-rich hydroxyapatite

The X-ray diffraction pattern of all samples was consistent with hydroxyapatite (from ICDD-entry 09-0432; Fig. 5). The chordacentra contain hydroxyapatite as their inorganic mineral phase and can therefore be regarded as bony tissue. The reflections of the samples are much broadened due to the nano-crystalline structure of hydroxyapatite. The calculated crystal sizes are shown in Table 1. It is notable that the mineral crystals are elongated along the crystallographic c-direction and thinner in the crystallographic a/b-direction, as in human and mouse bone. These particle shapes are not distinguishable crystallographically from human or mouse bone. The carbonate content of the hydroxyapatite of the chordacentra was about twice as high as in the adult vertebral body (Table 3). It was also twice the level found in mouse bone. The reference bones contained a higher amount of water, and the mouse bone had a higher and the human bone a lower degree of mineralization than the salmon samples.

Molecular fingerprints of the cellular core of the notochord

To determine whether collagen I or II was the dominating structural collagen of the notochord, the relative expression of their corresponding alpha-1/2 chain coding gene (*col2a1* and *col1a2*, respectively) were measured in the cellular core of the notochord (Fig. 6A). It was shown that type II collagen was the most highly expressed collagen, with about 1200 times the expression than of type I collagen (Fig. 6A). Both *col2a1* and the *collagen type XI α1* (*col11a1*) transcripts were likewise detected in the cellular core of the notochord and were observed to be significantly down-regulated at initiation of mineralization around 710 d° (Fig. 6B). Several signalling molecules and receptors have previously been associated with ECM formation and mineralization. To

monitor any activity of this sort, a number of key molecules, *sonic hedgehog* (*shh*), *indian hedgehog homolog b* (*ihhb*), *parathyroid hormone 1 receptor* (*pth1r*) and *transforming growth factor beta 1* (*tgfb1*) were measured in the notochord before and during early mineralization of the notochord. Both *shh* and *ihhb* were significantly down-regulated at the stage immediately before the onset of notochord mineralization. At the onset of mineralization (710 d°), expression levels *shh*, *tgfb1* and *pth1r* were significantly induced (Fig. 6C).

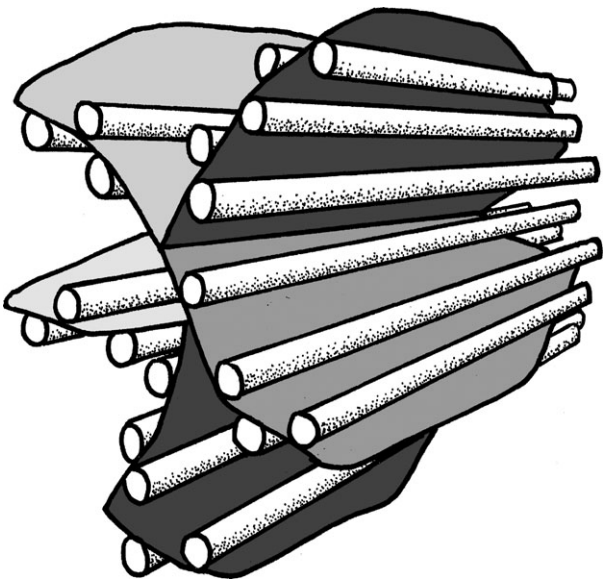

Fig. 3 Schematic drawing of the relationship between an early hydroxyapatite aggregate and collagen fibrils. This model holds for the mineralization of both lamellar type I and type II collagen matrices in salmon.

Discussion

Collagen modelling of the notochord and morphogenesis of the chordacentrum

The significantly higher gene expression of the type II collagen (*col2a1*) compared with the type I collagen (*col1a2*) in the cellular core of the salmon notochord confirms that the morphologically homogeneous collagen fibrils of the salmon notochord sheath seen with TEM are type II collagen fibrils. The collagen proteins are assembled in the notochord sheath, as little extracellular matrix is present in the cellular core. The three bony elements appearing in the notochord sheath, and subsequent fusion of these elements into a ring-shaped acellular chordacentrum, suggests a process regulated by positional signals from complex genetic networks. During chordacentrum formation, the major collagen (collagen type II, *col2a1*) and the minor collagen (collagen type XI, *col11a1*) were down-regulated. The reduction in structural collagens may affect the properties of the collagen matrix (Wenstrup et al. 2004; Olsvik et al. 2005), while the ratios between collagen II and XI may result in structural changes that which affect the three-dimensional architecture of the collagen fibrils (Blaschke et al. 2000); both aspects may have an influence on the process of mineralization. The reduced total collagen deposition accords with the view that the barrier imposed by the chordacentrum prevents further expansion of the notochord and its sheath. The capacity of the notochord cells (chordoblasts) to produce extracellular matrix that contributes to growth and reinforcement of initial vertebral bodies may therefore be restricted. Further growth of the vertebrae is achieved by recruitment of cells from the adjacent somite-derived sclerotomes (Fig. 7). The ring-shaped

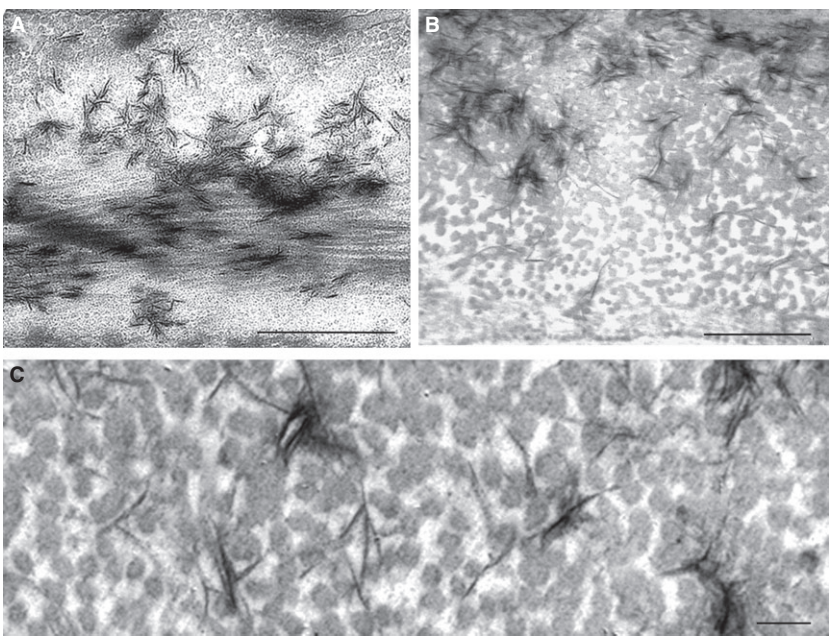

Fig. 4 Mineralization in the bone from the sclerotome-derived (type I collagen) part of the vertebral body (autocentrum). Transmission electron micrographs. (A) Two fibril layers, circular fibrils (upper part) and longitudinal fibrils, lower part. Note star-shaped aggregates in the upper region and the more diffuse aggregates in the lower part, showing the orientation of the plates along the collagen fibrils. Scale bar: 1 μm. (B,C) Higher magnifications show transversely sectioned collagen fibrils in the circular layer. Note the electron-dense mineral platelets that largely lie between and along the collagen fibrils. Scale bars: 500 nm (B), 100 nm (C).

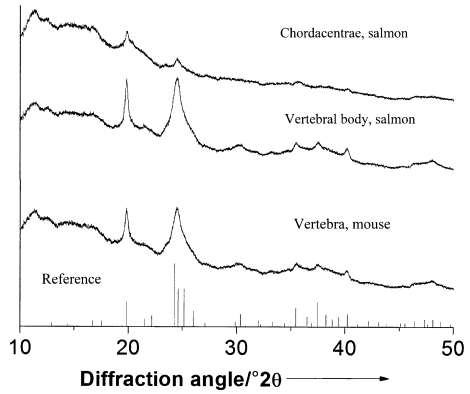

Fig. 5 Diffractograms of chordacentra and mature vertebral bodies of salmon compared with mouse bone. All diffractograms show the same peaks at the same positions.

Table 3 Content (in wt%) of water, organic matrix, carbonate, total mineral (carbonated hydroxyapatite), carbon dioxide and carbonate in the notochord centra and vertebral body of Atlantic salmon. Mouse and human bone were used as reference tissues.

	Water	Organic matrix	Total mineral	Carbon dioxide	Carbonate
Notochord centra	4.6	18.1	77.3	5.8	7.9
Vertebral body	4.3	21.1	74.6	2.7	3.7
Mouse bone	7	19.2	73.8	2.1	2.8
Human bone*	6.9	47.7	45.4		1.4

*Peters et al. (2000).

chordacentrum (Fig. 7A) acts as a foundation for the initial layer of the perinotochordal tissue. It is covered first by a layer with longitudinally oriented collagen fibrils, followed by a layer of fibrils in circular fashion (Fig. 7B,C). After the formation of the chordacentrum, its 400-μm diameter is unchanged during the rest of the growth process of the vertebral body (Fig. 7D,E) and in the adult stage the chordacentrum remains a separate entity in the middle of the vertebra (Fig. 7F).

The lamellarly arranged collagen fibrils provide an oriented support for crystal growth

The embryonic origin and composition of the collagen in the two extracellular matrices differed. The primary properties of the notochord sheath, when it initially forms, are adapted to fulfil specific functions related to locomotion during the early life stages. Thus, to trigger mineralization, new components that facilitate this mineralization process must be incorporated in a secondary process. The morphogenesis of the chordacentra is initiated by the generation

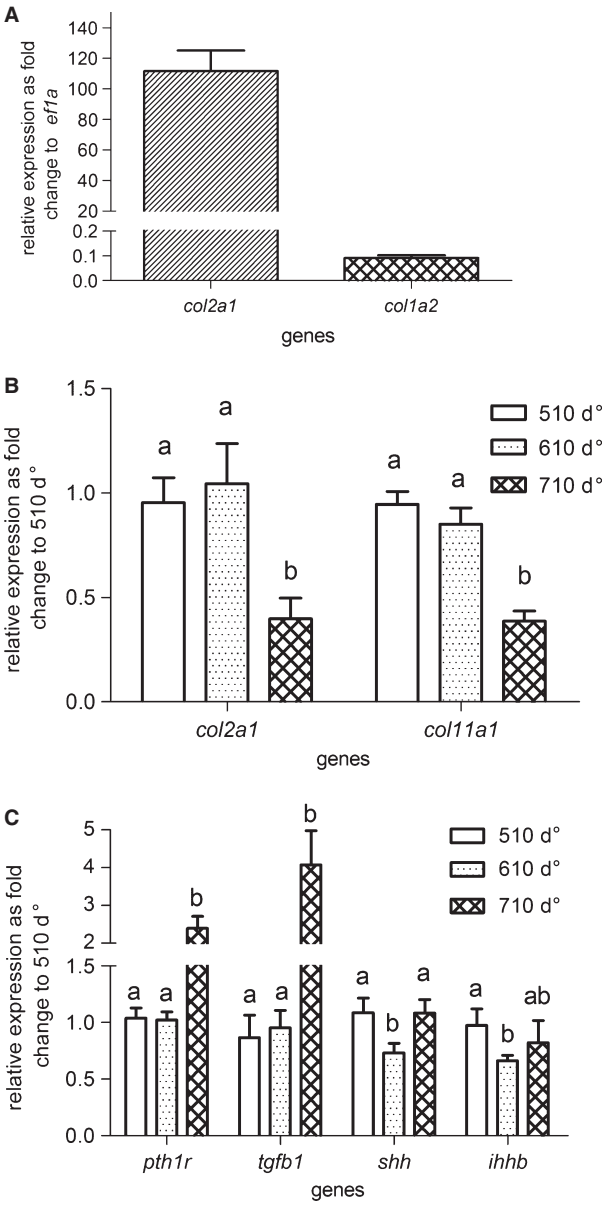

Fig. 6 Relative gene expression using qPCR at selected developmental stages (510, 610 and 710 d°). The relative expression of collagens *col2a1* and *col1a2* as fold change to reference gene *ef1a* in all stages (A). Relative expression of collagens *col2a1* and *col11a1* (B) and signalling genes *pth1r*, *tgfb1*, *shh* and *ihhb* (C) grouped by developmental stages as fold change to 510 d°. In pairwise comparison within one gene, a and b indicate a significant difference ($P < 0.01$), whereas ab shows that there was no significant differences from either a or b. Error bar indicates mean ± SD.

of prospective vertebral and intervertebral segments within the chordoblast layer (Grotmol et al. 2003). Indeed, this may be reflected by the segmentally arranged chordoblasts that develop osteoblast-like properties by expressing *alkaline phosphatase* (*alp*) (Grotmol et al. 2005; Bensimon-Brito et al. 2012) and *osteocalcin* (Bensimon-Brito et al. 2012). In the present study we demonstrate the expression of

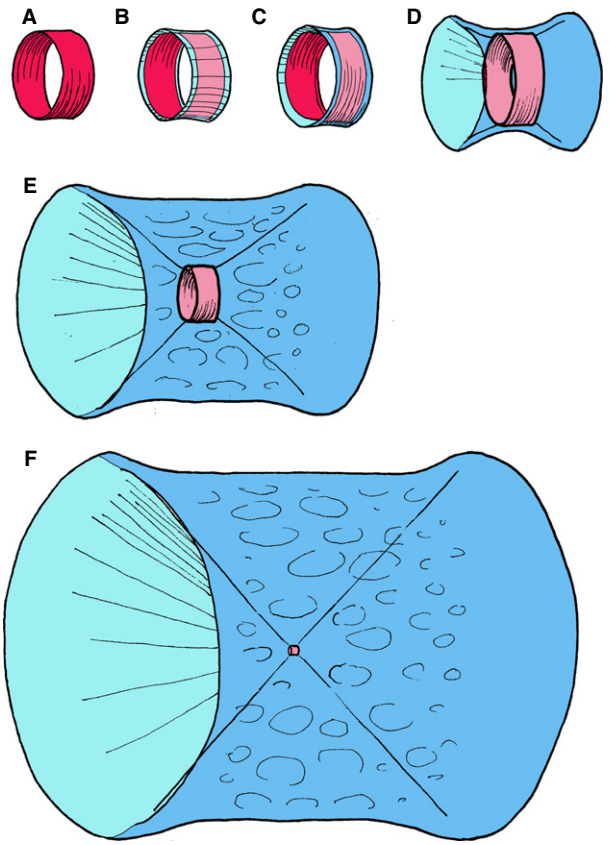

Fig. 7 Schematic drawings to illustrate the incorporation of the embryonic chordacentrum into the adult vertebra in Atlantic salmon. The ring-shaped chordacentrum (A) inside the notochordal sheath will retain its 400-μm diameter throughout the life cycle of the salmon. It is covered first by longitudinally (B) and then by circularly (C) oriented layers of collagen fibrils of sclerotomal origin. Further growth (D,F) of the vertebral body occurs only in this region, and the original template, the chordacentrum, remains as a narrow funnel in the middle of the vertebra.

multiple factors in the cellular core of the notochord known to be involved in the regulation of skeletogenesis. In the second step in the formation of the vertebral bodies the chordacentrum merges with bone produced by type I collagen fibril-secreting osteoblasts derived from the sclerotomes (Grotmol et al. 2005, 2006). In this part of the vertebral body, the organic matrix, secreted as osteoid, becomes mineralized shortly after secretion, implying that the components necessary to induce initiation and accretion, in a highly controlled manner, inherit properties of the matrix itself, once secreted. In spite of the ontogenetical difference, the nucleation, accretion and growth of the apatite had similar morphologies in the two collagen matrices studied.

The hydroxyapatite crystals grow parallel to the long axis of the collagen fibrils in both the type II and type I collagen matrices, thus affecting the three-dimensional architecture of the collagen fibrils. The lamellarly arranged collagen fibrils provide an oriented support for crystal growth. The assembly of the collagenous organic matrix prior to mineralization may therefore be the key step during the process of mineralization. The parallel arrangement of the collagen fibrils also ensures that the hydroxyapatite crystals form lamellar stacks rather than being randomly orientated.

In carbonate-rich hydroxyapatite, carbonate ions have probably replaced phosphate ions in the crystal, as is typical for bone mineral (Dorozhkin & Epple, 2002). The functional significance of the high carbonate content in the hydroxyapatite of the chordacentrum is not known. Salmon bone material mineral and mammalian bone mineral are crystallographically and chemically almost indistinguishable; in both cases hydroxyapatite is a carbonated, nano-sized crystal elongated along the crystallographic c-direction.

Collagen fibrils may provide regularly spaced templates for hydroxyapatite nucleation

Although the involvement of collagen in bone hydroxyapatite mineralization is generally recognized, its specific role remains unclear. It might be assumed *a priori* that at high resolution it should be possible to observe the presence of matrix vesicles and crystals therein, in addition to mineralized collagen fibrils and crystals in the interfibrillar space, and thus the initial mineral placement and the subsequent sequence of crystal accretion and attainment of habit should also be observable. In our study, no matrix vesicles were observed either in the notochord sheath or in the mineralizing osteoid secreted by the sclerotome-derived osteoblasts. Nor were mineralized collagen fibrils observed, either in type I or type II collagen fibrils, suggesting that in salmon the initial apatite nucleation and accretion are not confined to the gap regions between the collagen molecules, as has been hypothesized for some species (Veis, 2003). Furthermore, based on the average salmon apatite crystal diameter (which is about 21 nm) and the diameter of the salmon collagen fibrils (about 15 nm and 30–40 nm in type II and type I, respectively; Grotmol et al. 2006), it is difficult to imagine how crystals can fit into the gap region, suggesting that nucleation and growth are not confined to the 'intermolecular spaces' as hypothesized in one of the main models (Veis, 2003).

In the early phase of mineralization, we found non-mineralized collagen regularly spaced along the apatite crystal plates, suggesting that the apatite nucleates and accretes on the surface of the collagen fibrils and that the fibrils themselves control the orientation of the crystals. Multiple sources both *in vitro* and *in vivo* support the view that type I collagen plays a crucial role in the onset and progression of apatite mineralization (Schmitt, 1956; Landis & Silver, 2009; Wang et al. 2012). We have shown that the type II collagen fibril matrix may also mediate hydroxyapatite nucleation and that the crystals accrete a complex structure that reflects the direction of the fibrils in a pattern closely similar to that of the type I collagen matrix. Our

results are in accordance with the view that the apatite nucleation and growth are regulated by mineral–matrix interactions that provide regularly spaced templates or nucleation centres that determine the spatial relationship between the hydroxyapatite mineral and the collagen fibrils (Sasaki et al. 2002; Hall, 2005). Our results also agree with *in vitro* studies (Wang et al. 2012) that indicate that collagen fibrils can initiate and orient the growth of hydroxyapatite mineral in the absence of any other vertebrate extracellular matrix molecules of calcifying tissues, suggesting that the collagen fibril itself not only provides a template for the nucleation events for mineral formation but may also control the size and the three-dimensional distribution of hydroxyapatite on larger length scales. Our study indicates that the mineralization outside the fibrils can occur before and even in the absence of the long-recognized intrafibrillar mineralization.

Signalling molecule transcripts are expressed in the cellular core of notochord during the early mineralization process

During the early stage, the notochord secretes factors that provide positional and fate information for a variety of adjacent tissues (Gorski, 2011). Several zebrafish laminin and coatomer mutants show sharply distinct notochord sheath phenotypes and grafting experiments with dorsal organizers suggests that these key structural molecules are supplied by notochord cells (Coutinho et al. 2004; Stemple, 2005). Our study clearly shows that the notochord actively not only produces and maintains the notochord sheath but also expresses factors known to regulate osteogenesis and chondrogenesis, such as *shh, ihhb*, *tgfb1, pth1r* (Fig. 6C). Both *ihh* and *shh* have been shown previously to be expressed in the notochord of zebrafish (Krauss et al. 1993; Currie & Ingham, 1996; Stemple, 2005). Likewise their transcripts were identified in salmon notochord in this study. Both transcripts also contribute to the initiation of chondrocyte hypertrophy through PTHrP signal pathways (Karp et al. 2000; Karsenty, 2003). It is not clear why both *ihh* and *shh* expression should be reduced prior to the onset of mineralization. This reduction may also be related to the functions of these morphogens in stimulating the surrounding tissue (St-Jacques et al. 1999; Chung et al. 2001; Dahia et al. 2012). If chordocytes in the notochord resemble chondrocyte-like cells, the presence and regulation of both *ihh* and *pthr* in the notochord could be related to both mineralization and proliferation in chordocytes. The current view is that Ihh is an important paracrine regulator which can stimulate chondrocyte proliferation and inhibit maturation together with PTHrP and thereby contribute to increase both extracellular matrix deposition and mineralization (Kronenberg, 2003). Furthermore, the co-regulated induction of *shh, tgfb1* and *pth1r* at 710 d°, occurs at the onset of notochord mineralization. Consistent with this, in chondrocytes, hedgehogs are dependent on TGF-β signalling to induce PTH signalling (Alvarez et al. 2002). Moreover, a link between hedgehogs and pth has been identified in zebrafish (Bhattacharya et al. 2011). Several studies have also shown that these factors are co-expressed in chondrocytes at similar stages (Lanske et al. 1996). The dominant pth receptor in zebrafish (*pth2r*) has also been identified in the notochord of zebrafish, suggesting that salmon *pth1r* does indeed play a role in the notochord during mineralization of the notochordal sheath.

Formation of chordacentra may reflect a selectively advantageous evolutionary transition

The appearance of the notochord-derived chordacentra as mineralized segmental enforcements of the notochord sheath and the subsequent deposition of vertebral bone around these, probably reflect an evolutionary transition that provided dispersion and stabilization of tensile forces from the myosepta, acting along the cranio-caudal axis of the notochord. This probably proved selectively advantageous compared with enlargement of a persistent notochord alone. Chordacentra, similar to those we have described in salmon, have also been found in fossil lungfish-like osteichthyans from the Devonian (Janvier, 1996), which points towards the presence of notochord-derived metamerism as a key developmental mechanism that is also present in the sarcopterygian lineage, within which tetrapods have evolved. This raises the possibility that alternating mineral bodies and intervertebral discs in amniotes may likewise be influenced by metameric genetic signalling pathways within the notochord that position the chordacentra. This is consistent with the well documented persistence of notochord cells that form the nucleus pulposus of the intervertebral disc (Choi et al. 2008; Lefebvre & Bhattaram, 2010). Indeed, Stern (1990) has suggested that the notochord may be the archetypal structure of segmented vertebrae, perhaps including basal chordates. However, recent studies of segmentation in chick embryo, aimed at determining whether the notochord influences segmental vertebral patterning, exclude such a mechanism in avians, suggesting that this has been lost in the evolutionary transition (Senthinathan et al. 2012).

Acknowledgements

This work was funded by the Research Council of Norway. We gratefully acknowledge the expert help of Marine Harvest at Tveitevågen, Askøy, EWOS at Lønningdal Norway and Firda Seafood, Norway in rearing the salmon embryo and larvae. Expert technical assistance was provided by Teresa Cieplinska and Nina Ellingsen.

Author contributions

Study design: H.K., S.G., A.W., M.E., G.K.T. Conducting the study: H.K., S.G., A.W., G.K.T. Data collection: S.W., H.K.,

C.K., M.E., F.N. Data analysis: S.W., H.K., A.W., C.K., M.E., F.N., G.K.T.. Data interpretation: S.W., M.E., F.N., T.F.. Drafting manuscript: S.W., H.K., A.W., C.K., M.E., G.K.T. Approving final version of manuscript: S.W., H.K., A.W., C.K., M.E., G.K.T.

References

Abbink W, Glik G (2007) Parathyroid hormone-related protein in teleost fish. *Gen Comp Endocrinol* **152**, 243–251.

Adams DS, Keller R, Koehl MAR (1990) The mechanics of notochord elongation, straightening and stiffening in the embryo of *Xenopus laevis*. *Development* **110**, 115–130.

Alvarez J, Sohn P, Zeng X, et al. (2002) TGFbeta2 mediates the effects of hedgehog on hypertrophic differentiation and PTHrP expression. *Development* **129**, 1913–1924.

Anderson H, Garimella R, Tague SE (2005) The role of matrix vesicles in growth plate development and biomineralization. *Front Biosci* **10**, 822–837.

Becker A, Epple M, Müller KM, et al. (2004) A comparative study of clinically well-characterized human atherosclerotic plaques with histological, chemical, and ultrastructural methods. *J Inorg Biochem* **98**, 2032–2038.

Bensimon-Brito A, Cardeira J, Cancela ML, et al. (2012) Distinct patterns of notochord mineralization in zebrafish coincide with the localization of Osteocalcin isoform 1 during early vertebral centra formation. *BMC Dev Biol* **12**, 28.

Bhattacharya P, Yan YL, Postlethwait J, et al. (2011) Evolution of the vertebrate pth2 (tip39) gene family and the regulation of PTH type 2 receptor (pth2r) and its endogenous ligand pth2 by hedgehog signalling in zebrafish development. *J Endocrinol* **211**, 187–200.

Blaschke UK, Eikenberry EF, Hulmes DJ, et al. (2000) Collagen XI nucleates self-assembly and limits lateral growth of cartilage fibrils. *J Biol Chem* **275**, 10370–10378.

Bonucci E (2012) Bone mineralization. *Front Biosci* **17**, 100–128.

Boskey AL (2007) Mineralization of bones and teeth. *Elements* **3**, 387–393.

Choi K-S, Cohn MJ, Harfe BD (2008) Identification of nucleus pulposus precursor cells and notochordal remnants in the mouse: implications for disk degeneration and chordoma formation. *Dev Dyn* **237**, 3953–3958.

Chung UI, Schipani E, McMahon AP, et al. (2001) Indian hedgehog couples chondrogenesis to osteogenesis in endochondral bone development. *J Clin Invest* **107**, 295–304.

Coutinho P, Parsons MJ, Thomas KA, et al. (2004) Differential requirements for COPI transport during vertebrate early development. *Dev Cell* **7**, 547–558.

Currie PD, Ingham PW (1996) Induction of a specific muscle cell type by a hedgehog-like protein in zebrafish. *Nature* **382**, 452–455.

Dahia CL, Mahoney E, Wylie C (2012) Shh signaling from the nucleus pulposus is required for the postnatal growth and differentiation of the mouse intervertebral disc. *PLoS ONE* **7**, e35944.

Dorozhkin SV, Epple M (2002) Biological and medical significance of calcium phosphates. *Angew Chem Int Ed Engl* **41**, 3130–3146.

Eikenberry EF, Childs B, Sheren SB, et al. (1984) Crystalline fibril structure of type II collagen in lamprey notochord sheath. *J Mol Biol* **176**, 261–277.

Fleming A, Keynes R, Tannahill D (2004) A central role for the notochord in vertebral patterning. *Development* **131**, 873–880.

Glimcher MJ (2006) Bone: nature of the calcium phosphate crystals and cellular, structural, and physical chemical mechanisms in their formation. *Rev Mineral Geochem* **64**, 223–282.

Gorski JP (2011) Biomineralization of bone: a fresh view of the roles of non-collagenous proteins. *Front Biosci* **16**, 2598–2621.

Grotmol S, Kryvi H, Nordvik K, et al. (2003) Notochord segmentation may lay down the pathway for the development of the vertebral bodies in the Atlantic salmon. *Anat Embryol (Berl)* **207**, 263–272.

Grotmol S, Nordvik K, Kryvi H, et al. (2005) A segmental pattern of alkaline phosphatase activity within the notochord coincides with the initial formation of the vertebral bodies. *J Anat* **206**, 427–436.

Grotmol S, Kryvi H, Keynes R, et al. (2006) Stepwise enforcement of the notochord and its intersection with the myoseptum: an evolutionary path leading to development of the vertebra? *J Anat* **209**, 339–357.

Hall BK (2005) The Search for the Magic Bullet. In: *Bones and Cartilage: Developmental and Evolutionary Skeletal Biology*. (ed. Hall BK), pp. 525–526, London: Elsevier Academic Press.

Huq NL, Cross KJ, Ung M, et al. (2005) A review of protein structure and gene organisation for proteins associated with mineralised tissue and calcium phosphate stabilisation encoded on human chromosome 4. *Arch Oral Biol* **50**, 599–609.

Janvier P (1996) *Early Vertebrates*. Oxford: Clarendon Press.

Karp SJ, Schipani E, St-Jacques B, et al. (2000) Indian hedgehog coordinates endochondral bone growth and morphogenesis via parathyroid hormone related-protein-dependent and -independent pathways. *Development* **127**, 543–548.

Karsenty G (2003) The complexities of skeletal biology. *Nature* **423**, 316–318.

Knapp M, Baehtz C, Ehrenberg H, et al. (2004a) The synchrotron powder diffractometer at beamline B2 at HASYLAB/DESY: status and capabilities. *J Synchrotron Radiat* **11**, 328–334.

Knapp M, Joco V, Baehtz C, et al. (2004b) Position-sensitive detector system OBI for high resolution X-ray powder diffraction using on-site readable image plates. *Nucl Instr Methods Phys Res* **521**, 565–570.

Koehl MAR, Quillin K, Pell C (2000) Mechanical design of fiber-wound hydraulic skeletons: the stiffening and straightening of embryonic notochords. *Am Zool* **40**, 28–41.

Krauss S, Concordet JP, Ingham PW (1993) A functionally conserved homolog of the Drosophila segment polarity gene *hh* is expressed in tissues with polarizing activity in zebrafish embryos. *Cell* **75**, 1431–1444.

Kronenberg HM (2003) Developmental regulation of the growth plate. *Nature* **423**, 332–336.

Landis WJ, Silver FH (2009) Mineral deposition in the extracellular matrices of vertebrate tissues: identification of possible apatite nucleation sites on type I collagen. *Cells Tissues Organs* **189**, 20–24.

Lanske B, Karaplis AC, Lee K, et al. (1996) PTH/PTHrP receptor in early development and Indian hedgehog-regulated bone growth. *Science* **273**, 663–666.

Lefebvre V, Bhattaram P (2010) Vertebrate skeletogenesis. *Cur Top Dev Biol* **90**, 291–317.

Nordvik K, Kryvi H, Totland GK, et al. (2005) The salmon vertebral body develops through mineralization of two preformed tissues that are encompassed by two layers of bone. *J Anat* **206**, 103–114.

Olsvik PA, Lie KK, Jordal A-EO, et al. (2005) Evaluation of potential reference genes in real-time RT-PCR studies of Atlantic salmon. *BMC Mol Biol* **17**, 6–21.

Peters F, Schwarz K, Epple M (2000) The structure of bone studied with synchrotron X-ray diffraction, X-ray absorption spectroscopy and thermal analysis. *Thermochim Acta* **361**, 131–138.

Qin C, Baba O, Butler WT (2004) Post-translational modifications of sibling proteins and their roles in osteogenesis and dentinogenesis. *Crit Rev Oral Biol Med* **15**, 126–136.

Sagstad A, Grotmol S, Kryvi H, et al. (2011) Identification of vimentin- and elastin-like transcripts specifically expressed in developing notochord of Atlantic salmon (*Salmo salar* L.). *Cell Tissue Res* **346**, 191–202.

Sasaki N, Tagami A, Goto T, et al. (2002) Atomic force microscopic studies on the structure of bovine femoral cortical bone at the collagen fibril-mineral level. *J Mater Sci Mater Med* **13**, 333–337.

Schmitt F (1956) Macromolecular interaction patterns in biological systems. *Proc Am Philos Soc* **100**, 476–486.

Senthinathan B, Sousa C, Tannahill D, et al. (2012) The generation of vertebral segmental patterning in the chick embryo. *J Anat* **220**, 591–602.

Stemple DL (2005) Structure and function of the notochord: an essential organ for chordate development. *Development* **132**, 2503–2512.

Stern CD (1990) Two distinct mechanisms for segmentation? *Semin Dev Biol* **1**, 109–116.

St-Jacques B, Hammerschmidt M, McMahon AP (1999) Indian hedgehog signaling regulates proliferation and differentiation of chondrocytes and is essential for bone formation. *Genes Dev* **13**, 2072–2086. Erratum in: Genes Dev 13, 2617.

Veis A (2003) Mineralization in organic matrix frameworks. *Rev Mineral Geochem* **54**, 249–289.

Wang Y, Azaïs T, Robin M, et al. (2012) The predominant role of collagen in the nucleation, growth, structure and orientation of bone apatite. *Nat Mater* **11**, 724–733.

Wargelius A, Fjelldal PG, Nordgarden U, et al. (2010) *Collagen type XI* (α1) may be involved in the structural plasticity of the vertebral column in Atlantic salmon (*Salmo salar* L.). *J Exp Biol* **213**, 1207–1216.

Wenstrup RJ, Smith SM, Florer JB, et al. (2004) Regulation of collagen fibril nucleation and initial fibril assembly involves coordinate interactions with collagens V and XI in developing tendon. *J Biol Chem* **279**, 53331–53337.

Yu B, Zhao X, Yang C, et al. (2012) Parathyroid hormone induces differentiation of mesenchymal stromal/stem cells by enhancing bone morphogenetic protein signalling. *J Bone Miner Res* **27**, 2001–2014.

Zhu W, Robey PG, Boskey AL (2008) The regulatory role of matrix proteins in mineralization of bone. In: *Osteoporosis*. (eds Marcus R, Feldman D, Nelson D, Rosen C), 3rd edn, pp. 191–240, New York: Elsevier.